15

# Muonography of the structure of the power unit of the Kalinin NPP

© N.A. Pasyuk,[1] R.R. Alyev,[2] N.N. Davidenko,[3] S.M. Kiselev,[2] A.S. Kozhin,[1,4] K.G. Kompaniets,[1] Yu.N. Konev,[3] S.V. Oleinik,[3] A.A. Petrukhin,[1] R.M. Fakhrutdinov,[1,4] M.Yu. Tselinenko,[1] V.V. Shutenko,[1] I.I. Yashin[1]

[1] National Research Nuclear University „MEPhI“,
115409 Moscow, Russia
[2] Branch of JSC „Rosenergoatom Concern“ „Kalinin Nuclear Power Plant“,
171841 Udomlya, Tver region, Russia
[3] All-Russian Research Institute for the Operation of Nuclear Power Plants,
109507 Moscow, Russia
[4] Federal State Budgetary Institution "Institute of High Energy Physics named after A.A. Logunov, National Research Center „Kurchatov Institute“,
142281 Protvino, Moscow region, Russia
e-mail: NAPasyuk@mephi.ru

*Received August 9, 2024*
*Revised October 20, 2024*
*Accepted October 21, 2024*

A large-area hybrid muon hodoscope for studying the internal structure of large-scale objects using the muonography method was constructed at the National Research Nuclear University MEPhI in 2022–2023. The hodoscope detecting system has a hybrid structure and consists of a scintillation strip detector and a drift tube detector and is designed to record tracks of charged particles, mainly muons. Recording systems, data processing and particle track reconstruction methods have been developed for each detector. Experimental studies of the internal structure of the Kalinin NPP power unit using the muonography method were carried out in 2022–2023. A description of the design of the hybrid muon hodoscope, the method for constructing muonograms, as well as the results of the first experiment conducted under normal operating conditions of the power unit are presented in the article.

**Keywords:** cosmic ray muons, particle detectors, scintillation strips, scintillation detector, drift tubes, muon hodoscope, muonography, muonogram, nuclear reactor.

DOI: 10.61011/TP.2025.01.60523.251-24

## Introduction

The muon flux is formed in the upper atmosphere as a result of the interaction of protons and nuclei of primary cosmic rays, as well as secondary hadrons, with the nuclei of atmospheric atoms. Muons have significant penetrating power, since at a characteristic average energy at sea level from 4 to 100 GeV, depending on the zenith angle, they lose energy mainly to ionization. One of the features of the muon flux is the dependence of its intensity and average energy on the zenith angle (measured from the vertical): $I(\theta) = I(\theta_0) \cdot \cos^n \theta$, where the exponent $n = n(p)$ is a function of the momentum (energy) of the muons [1]. The ability of muons to penetrate through large masses of matter is employed by the methods of scanning of large-scale natural or industrial objects.

Analysis of changes in the spatial and angular distribution of muons during passage through a large-scale object can provide information about the mass composition and density distribution of the matter through which they pass. This method is called muonography (by analogy with radiography).

One of the first muonography methods was used by L.U. Alvarez in 1970 to search for hidden rooms in the Great Pyramid of Giza [2]. Currently, muonography is used for non-destructive testing and the creation of muonogram images using various imaging methods: from two-dimensional analysis using muon flux attenuation measurements to three-dimensional muon tomography based on multiple Coulomb scattering of muons as they pass through matter [3–5].

The muonography method is used to study various objects, including powerful turbulent phenomena in the Earth's atmosphere and magnetosphere (hurricanes, powerful thunderstorms, squalls, snowstorms) [6–8], pyramids [9,10], volcanoes [11,12], geological [13,14], archaeological [15,16] and industrial [17–20] objects, etc. Muonography plays an important role in the development of methods for controlling the movement of heavy fissile substances [21,22] and remote monitoring of reactors [23–25]. A special interest in muonography of nuclear reactors arose in connection with the accident at the Fukushima Daiichi Nuclear Power Plant [26–28]. The method of remote sensing of failed reactors using muons turned out to be the only one that was used to obtain estimates of the distribution of molten fuel inside the reactor zone.

Scientific & Educational Centre NEVOD (National Research Nuclear University MEPhI) in cooperation with JSC „VNIIAES“ (Rosatom) created and tested a mobile

hybrid muon hodoscope for development of methods for monitoring and non-destructive testing of large-scale facilities in real time, including nuclear power plants, using the muonography method [29]. This paper describes the features of the detecting and recording systems of the muon hodoscope, as well as discusses the results of the first experiment on muonography of a power unit with a VVER-1000 reactor at the Kalinin NPP (Udomlya), obtained in 2022 during its normal operation.

## 1. Hybrid muon hodoscope design

The hybrid muon hodoscope (HMH) [30] has a modular design and consists of two independent systems: a drift tube detector (DTD) [31] and the scintillation strip detector (SSD) [32]. Both detectors have their advantages and complement each other when working together. The scintillation detector is easy to operate, makes it possible to organize a fast trigger and quickly reconstruct the muon tracks. DTD provides one of the best coordinate resolutions of muon tracks, second only to nuclear emulsions.

The hodoscope (Fig. 1) consists of 10 alternating orthogonally oriented single-projection coordinate planes (SCP) with a sensitive area of $3 \times 3$ m each. Six planes make up the scintillation detector and four planes — DTD. DTD planes consist of three-layer assemblies of 288 drift tubes with a length of 3000 mm and a diameter of 30 mm [31,33]. The SSD planes consist of 128 long, narrow rectangular scintillation strips ($3000 \times 23 \times 7$ mm) with fiber-optic light collection on silicon photomultipliers (SiPM) [32,34]. The distance between the extreme SCP is 1.8 m.

All planes are combined in the main supporting frame, which is a box consisting of upper, lower and side straps (Fig. 1). The frame is mounted on a rotating platform

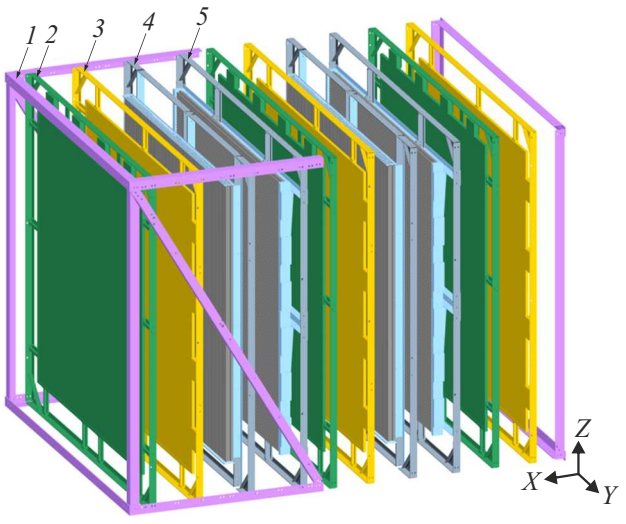


**Figure 1.** 3*D*-HMH model: *1* — main support frame; *2* — SSD plane with vertically oriented strips; *3* — SSD plane with horizontally oriented strips; *4* — DTD plane with vertically oriented tubes; *5* — DTD plane with horizontally oriented tubes.

**Figure 2.** Photo of HMH.

(Fig. 2) connected to a mobile module on a two-axle chassis with extendable supports. This ensures the mobility and convenience of the orientation of the entire structure relative to the studied object. By moving the HMH around the studied object and scanning it from several directions, it is possible to obtain a 3*D*-image (tomography). A DTD gas system with gas collectors is also mounted on the frame. The dimensions of the assembled HMH are 4.5 m in height, 2.5 m in width, 6.2 m in length. The mass of the assembled HMH is about 4.5 t.

The accuracy characteristics of the hodoscope were studied by the National Research Nuclear University MEPhI in 2022 using lead blocks placed at various distances and heights [35]. An angular accuracy of about 2 mrad was demonstrated when locating objects with a size of $40 \times 40 \times 40$ cm at a distance of up to 40 m.

Muonography experiments were conducted in Kalinin NPP power unit (Udomlya) using HMH in 2022–2023. The HMH was located at a distance of about 70 m from the center of the reactor on the site in a special pneumo-framed module (Fig. 3) with the size $8.2 \times 8.2$ m with a height of 6.4 m [36]. In addition to the pneumo-framed module and the HMH, the test bench included an equipment rack, gas cylinders, an electrical power supply system and a fire alarm system. The coordinate planes were tilted by 12° after the HMH was installed and secured to better capture the muon flux passing through the observed object.

**Figure 3.** Placement of the HMH relative to the power unit.

## 2. Method of constructing muonograms

A matrix is constructed on a plane perpendicular to the axis of the detector to obtain a muonogram. Each cell of this matrix contains information about the number of intersections of the reconstructed tracks passing through it. At the same time, local and laboratory coordinate systems are defined for the reconstruction of events in the HMH detectors and the subsequent construction of muonograms [35]. The use of two coordinate systems (Fig. 4) makes it easy to take into account the position of the detectors in space by moving and rotating the local coordinate system relative to the laboratory one. The laboratory coordinate system is represented by a right-hand rectangular system, the starting point of which is located in the corner of the supporting frame of the HMH.

Strips and tubes in a separate coordinate plane are oriented in a certain direction, coinciding with the direction of either $Y_{\text{lab}}$ (vertical) or $Z_{\text{lab}}$ (horizontal) axes of the laboratory coordinate system (Fig. 4). The axis $X_{\text{lab}}$ coincides with the axis of the detector, directed perpendicular to the coordinate planes in the direction of the studied object. The beginning of the local coordinate system in the SSD is tied to the coordinates of the first strips of the SCP, and to the coordinates of the first tubes of the drift chambers in the DTD.

Reconstruction of track parameters in detectors is based on its registration by several SCP [35]. Each coordinate plane provides information about the triggered channels, which allows estimating the coordinate of the point of intersection of the SCP assembly by the muon. The data of several coordinate planes with the corresponding orientation of the strips (tubes) allow the reconstruction of the track in the corresponding projection planes $XY$ and $XZ$. Information about the two projections makes it possible to reconstruct the track in three-dimensional space (Fig. 5). The methods of event reconstruction and construction of muonograms in HMH detectors are described in more detail in Ref. [35].

After reconstruction of the track, the point of its intersection with the reference plane is determined, set at a distance $L$ from the detector perpendicular to the axis $X$ of the laboratory coordinate system and passing through the studied object (Fig. 5). The dimensions of this plane $Y_L$ and $Z_L$ correspond to the search area of the studied object. The area of this plane, determined by the value $Y_L \times Z_L$, is divided into cells in increments $\Delta y$, $\Delta z$, forming a matrix $M$ of dimension $k = \text{int}(Y_L/\Delta y)$, $m = \text{int}(Z_L/\Delta z)$. The number of the corresponding cell of the matrix $M[i, j]$ hit by the muon track line drawn from the detector to the plane in the opposite direction to the track is determined when the track intersects the plane. The unit $M[i, j] = M[i, j] + 1$ is added to this cell of the matrix. Such a matrix represents a shadow image in a set of cells and displays the distribution of regions of inhomogeneities in the angular distribution of the recorded muon flux associated with the structural features of the observed object.

Comparison of the experimental matrices with the simulated muon flux passing through the HMH within the aperture without an object makes it possible to obtain muonograms (matrices taking into account the angular

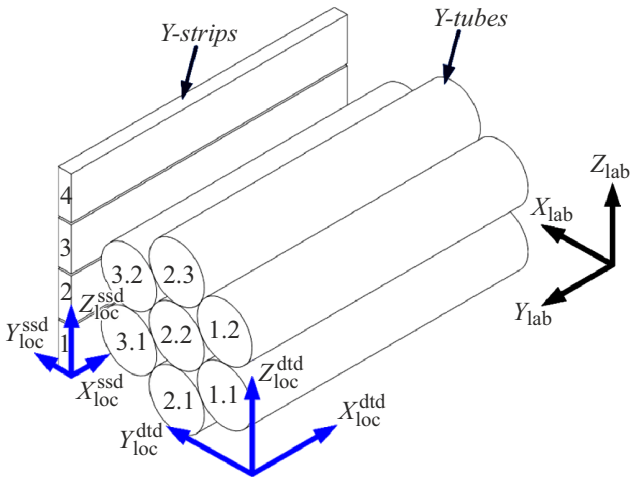


**Figure 4.** HMH coordinate system.

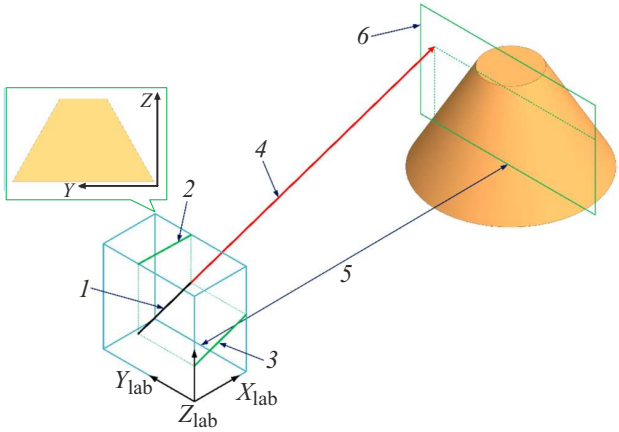


**Figure 5.** Muonogram construction scheme: *1* — reconstructed track; *2* — $XY$-projection; *3* — $XZ$-projection; *4* — projected track; *5* — distance to object; *6* — reference plane.

dependence of the muons) and calculated matrices of the thickness of the substance of the observed object. The thickness matrices provide an average estimate of the amount of matter traveled by the particles to the registration site. The particle flux, including muons, was calculated using modeling of extensive air showers from primary protons with energies from 1 to $10^4$ GeV in increments of $\Delta(\log_{10}(E_0)) = 0.1$. Software package CORSIKA version 7.7500 was used for modeling.

Protons were modeled in a standard atmosphere, taking into account its curvature in the range of zenith angles from 0 to 89° and in the range of azimuth angles from 0 to 360°. Observation level — 173 m. When modeling primary charged hadrons, ionization losses and deflection in the Earth's magnetic field were taken into account (according to IGRF2020 model dated 01.08.2023) on the way from atmospheric entry to the first interaction. Two models were used to describe hadron interactions: QGSJET-II-04 for high energy and FLUKAINFN2021.2.9 for low energies. The transition boundary between the models was 80 GeV.

The simulation includes several stages. At the first stage, random directions and positions of the particle track $T(x_1, y_1, z_1, x_2, y_2, z_2, \varphi, \theta)$ are modeled in the space of the laboratory coordinate system, where $x_1, y_1, z_1$ and $x_2, y_2, z_2$ — the start and end points of the track, and $\theta$ and $\varphi$ — zenith and azimuth directions. The tracks that intersect the reference plane and are located within the detector aperture are selected. Then the intersection of the track with the cells of the matrix $M[i, j]$ is determined on the reference plane. Knowing the cell area in the matrix $S$ and the distance to the reference plane, it is possible to calculate the solid angle $d\Omega$ of each cell and estimate the intensity of the flux of muons $[\text{cm}^{-2}\cdot\text{s}^{-1}\cdot\text{sr}^{-1}]$ per unit of time $dt$ taking into account the efficiency of registration $\varepsilon$:

$$I(S, \Omega) = \frac{dN}{dS \cdot d\Omega \cdot \varepsilon \cdot dt}. \quad (1)$$

After that, according to the corresponding cells of the matrix $M[i, j]$, a matrix of deviations $D[i, j]$ of the number of tracks in the experiment $N_{i,j}$ is determined relative to the number of tracks in the model $N_{0i,j}$, taking into account the normalization coefficient $B$: $D_{i,j} = N_{i,j}/(B \cdot N_{0,i,j})$, where $B = \Sigma_{i,j}(N_{i,j})/\Sigma_{i,j}(N_{0i,j})$. Using the calculated table of the dependence of the muon flux intensity on the zenith angle and threshold energy, for each cell of the experimental matrix, such threshold energy $E_{i,j}$ is determined at which the flux intensity would change by a factor of $D_{i,j}$ compared to the model threshold energy $E_{0i,j}$. This table was obtained on the basis of the calculated spectrum in CORSIKA using formulas from Ref. [37,38]. The thickness of the substance $X$, taking into account the minimum muon ionization losses of 2 MeV·g$^{-1}$·cm$^2$ is estimated as follows:

$$X_{i,j}[\text{g}\cdot\text{cm}^{-2}] = \frac{(E_{i,j} - E_{0i,j})[\text{MeV}]}{2.0[\text{MeV}\cdot\text{g}^{-1}\cdot\text{cm}^2]}. \quad (2)$$

## 3. Muonography of the NPP power unit

The duration of the muonography experiment at the Kalinin NPP, conducted in the fall of 2022, was 20 calendar days, during which 130 million tracks of single muons were reconstructed. The main purpose of the measurements was to monitor the power unit operating normally, to check the operability of the HMH system and to develop a methodology for obtaining muonograms.

Zenith-angular and azimuthal distributions of tracks with a step of 1° were obtained from the reconstructed events. Fig. 6 shows the distribution along the zenith angle in the forward direction (from the side of the power unit), and Fig. 7 — the distribution along the azimuth angle, where from 0 to 180° is the forward direction, and from 180 up to 360° is the reverse (on the other side of the detector). The angular aperture of the detector in the forward direction is 80° in the zenith angle and 160° in the azimuth angle. The figure clearly shows a decrease of the flow towards the power unit and the building from the opposite side. The obtained experimental angular distributions made it possible

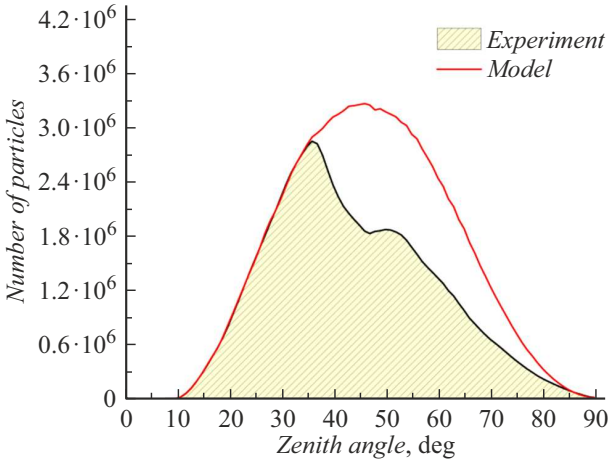


**Figure 6.** Distribution of the number of HMH tracks by zenith angle.

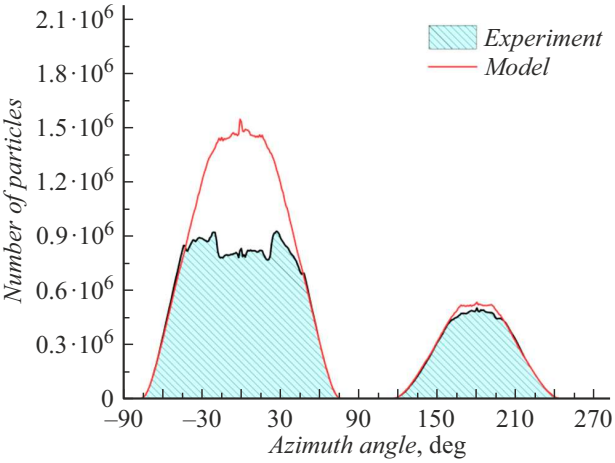


**Figure 7.** Distribution of the number of HMH tracks by azimuth angle.

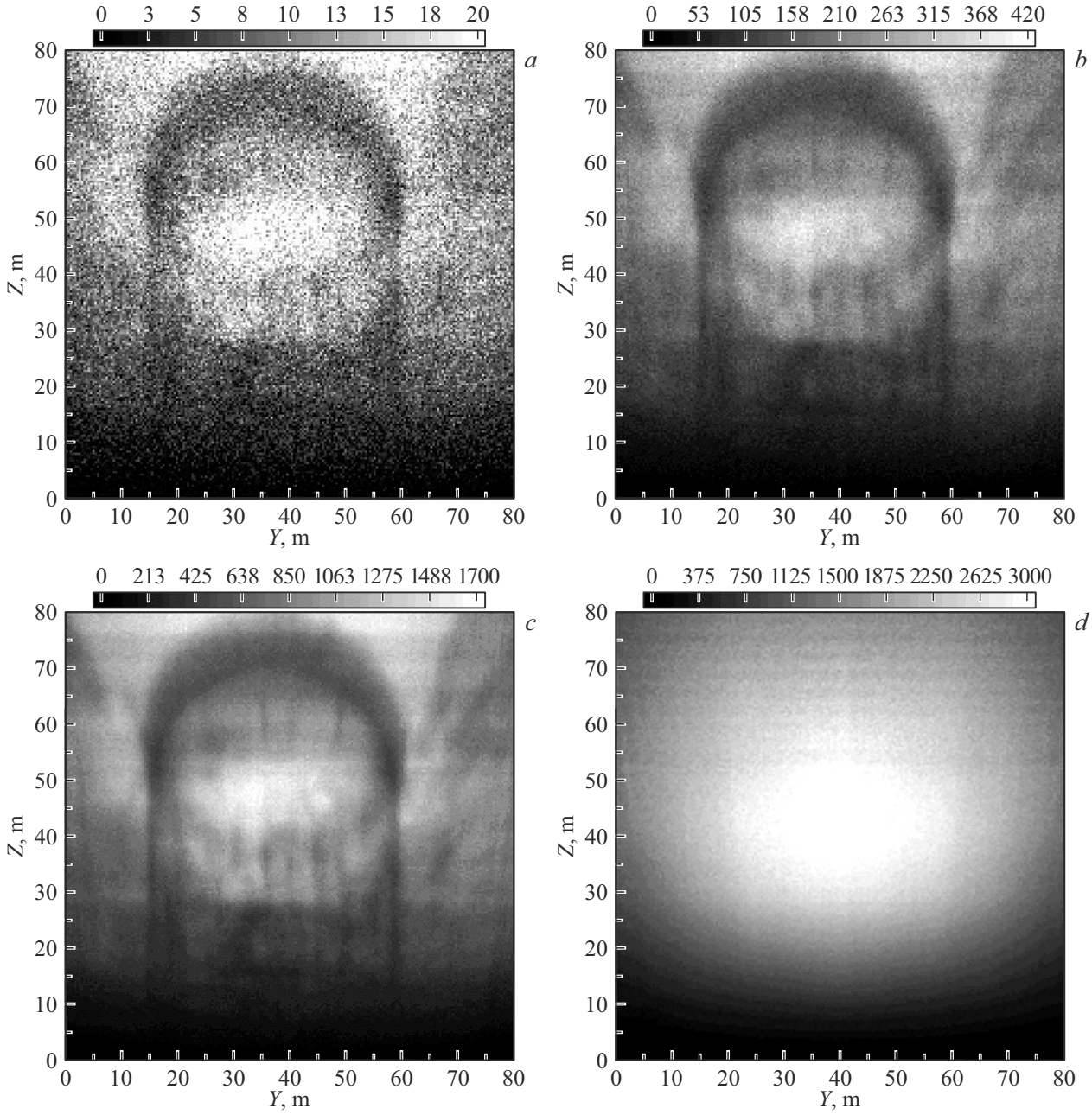


**Figure 8.** Track count matrices: *a* — 5 h; *b* — 5 days; *c* — 20 days; *d* — model.

to fine-tune the model muon spectrum by comparing the model and experiment in areas where the muon flux was not shielded by buildings. The model angular distributions without a power unit are shown by the red histogram in Fig. 6 and 7.

Fig. 8 shows the rate of formation of experimental muonograms. A model matrix without obstacles on the trajectory of the particles is also shown. The simulation was carried out using the particle spectrum obtained using the CORSIKA software package in the manner described above, followed by normalization to experimental data. The matrices were constructed at a distance of 60 m from the center of the detector and have dimensions $80 \times 80$ m with a cell resolution of $0.4 \times 0.4$ m. The boundaries of the containment and the reactor compartment structures appear after several hours of observation, and with an increase in the amount of data, the contrast of the image increases. The visual clarity of the image also depends on the selected color gradation and the size of the matrix cell. The blurriness of the image in the lower part is caused by a natural decrease of the muon flux and, as a result, a decrease of statistics.

The model matrix is used to normalize experimental data to account for and exclude the systematic impact of a

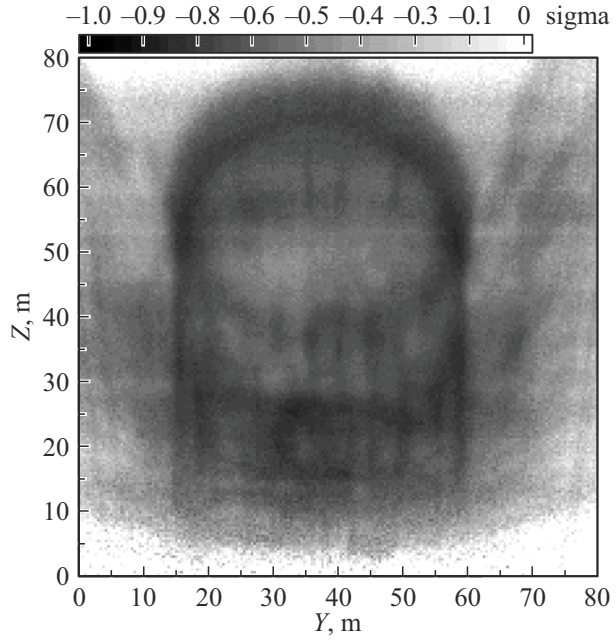


**Figure 9.** Deviation matrix.

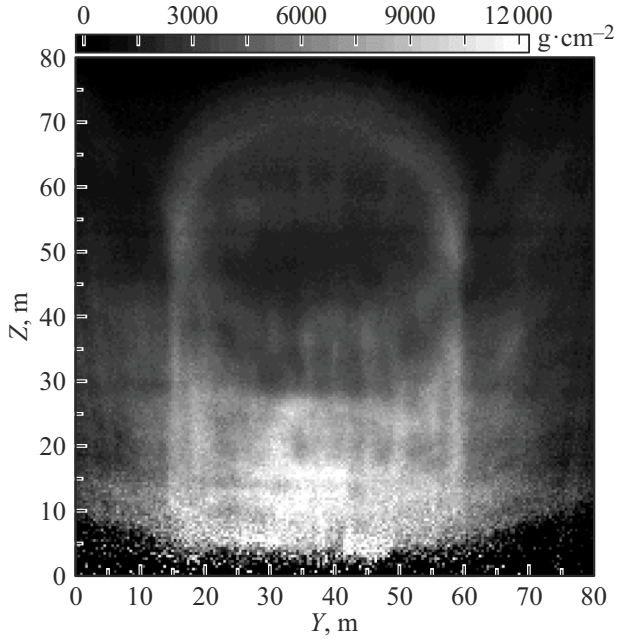


**Figure 10.** Thickness matrix.

strong angular dependence of the muon flux, which makes it possible to more accurately identify areas with anisotropy.

Fig. 9 shows a muonogram matrix obtained taking into account the statistics of registered muons with normalization to the model spectrum. Fig. 10 shows a matrix of substance thicknesses across the matrix cells. When comparing Fig. 9 and 8, *c*, it can be seen that the normalized matrix reflects in more detail the structural features of the power unit complex. The vertical stripes in the center of the image and „wings“ in the areas from 0 to 10 m and from 65 to 80 m along the axis $Y$ correspond to the concrete walls and ceilings of the auxiliary rooms of the reactor compartment. The reactor zone is located at a height from 15 to 35 m, and below 15 m, the reactor rooms, equipment and turbine complex of the engine room are projected.

## 4. Interpretation of muonograms of the NPP power unit

The image obtained by the HMH when observing an object at a certain angle to the horizon undergoes a promising transformation due to the construction of matrices based on tracks reconstructed at the projection angles $\Delta\varphi$ and $\Delta\theta$ of the detector, followed by projection in the opposite direction onto the reference plane. Fig. 11 clearly shows how the internal structure of a power unit with a VVER-1000 reactor is distorted in a muonogram obtained at a distance of 68 m from the detector. Distortions along the width of the image (axis $Y$) are minimal since the detector is horizontally positioned almost in the center of the reactor. Storage pools are along the axis $Y$ in the range from 17 to 32 m, reactor zone is between 32 and 41 m, refueling pools and turbine engine room are between 41 and 51 m, and auxiliary rooms are in the range from 5 to 17 m and from 55 to 70 m. The image stretches from bottom up in the vertical plane (axis $Z$). The engine room and floor slabs are projected along the axis $Z$ in the range from 0 to 15 m, reactor zone is projected between 15 and 35 m, and auxiliary and protective structures of the upper part of the containment are projected in range from 35 to 80 m.

It is possible to estimate the thickness of the walls of the containment of reactor building using muonograms. However, the problem lies in the fact that the objects through which the muons pass are shielded by a layer of matter equivalent to 10–12 m of concrete. An important role in shielding the reactor is played by 3 m thick horizontal sub-reactor concrete slab, located at a height of 10 m. The passage of muons through such a layer leads to multiple Coulomb scattering, which causes blurring of the contours of objects.

A vertical section of the containment wall was chosen to verify the accuracy of the measurements because of the lowest scattering of muons passing through it. Fig. 12 shows a muonogram and histograms for a horizontal section. The horizontal section at a height of 32 m was chosen due to the absence of large objects that could distort the measurement results. The step of the histogram was 20 cm. The measurements showed that the wall thickness is $120 \pm 20$ cm, which corresponds to the actual thickness. The outer edge of the wall was measured with a spatial accuracy of at least 10 cm, which corresponds to an angular resolution of 1.5 mrad. These results are in good agreement with the measurement data obtained using HMH prototype at MEPhI [35].

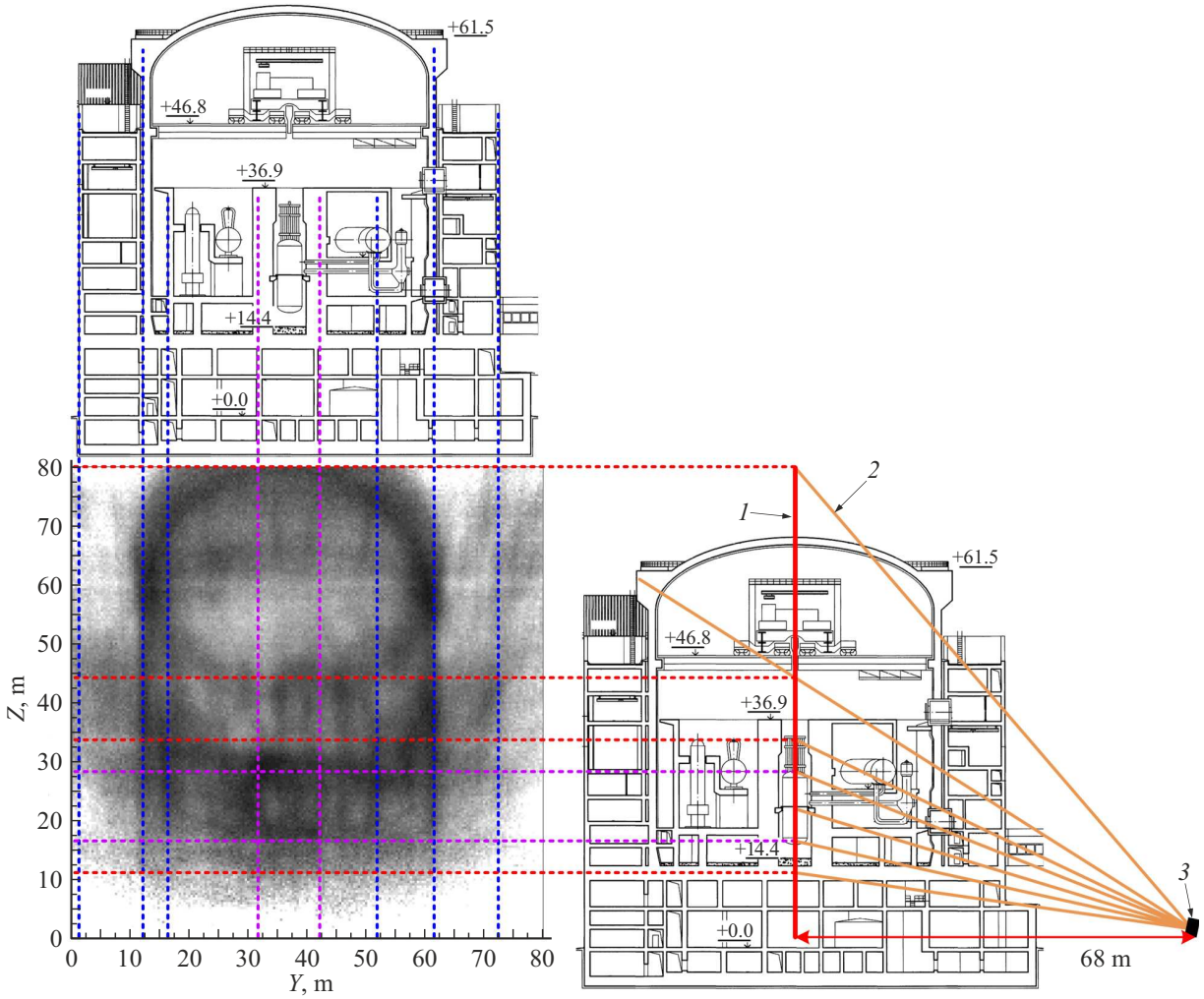


**Figure 11.** Muonogram formation scheme of the NPP power unit: *1* — reference plane; *2* — particle track; *3* — detector.

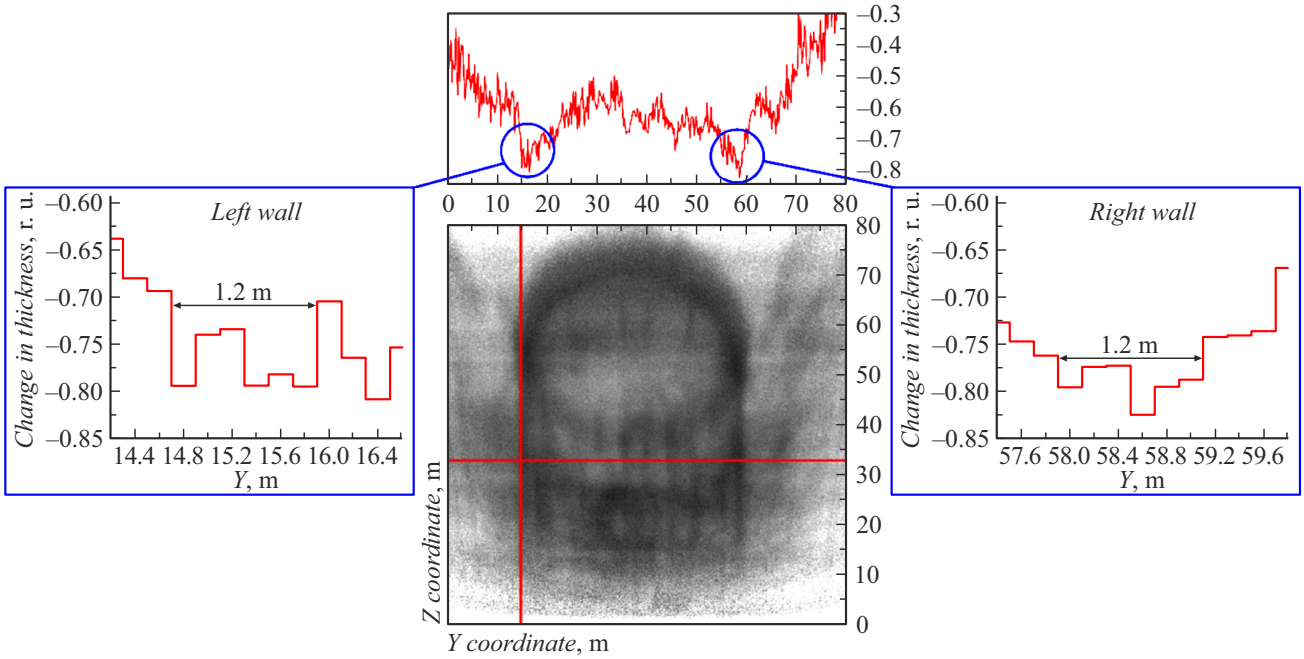


**Figure 12.** Measurement of the thickness of the walls of the power unit containment.

## Conclusion

The developed wide-aperture hybrid muon hodoscope was used to test the method of muonography of the operating power unit of the Kalinin NPP with the VVER-1000 reactor. The correct functioning of the hybrid muon hodoscope and its ability to receive muonograms were confirmed according to the results of the first experiment. It is important to note that the hodoscope installed outside the power unit demonstrated the possibility of visualizing the structure of a nuclear reactor unit.

The images obtained make it possible to identify various components of the power unit structure. However, the difficulty of identifying small objects, despite the good angular accuracy of the detector ($\sim 2$ mrad), is associated with large thicknesses of background concrete walls and floors ($10000-14000\,g/cm^2$), which are projected onto the studied objects. In addition, the boundaries of structures become less clear with insufficient statistics and due to multiple Coulomb scattering on dense structures of the power unit, especially in the lower part of the reactor.

### Acknowledgments

The authors would like to thank the staff of Scientific & Educational Centre NEVOD for valuable advice, fruitful discussion of the results and assistance in creating, testing and deploying HMH at Kalinin NPP, as well as the staff of Kalinin NPP and the branch of JSC „VNIIAES“ (Udomlya) for their assistance in conducting experimental research.

### Funding

The development and study of the hybrid muon hodoscope were carried out under the scope of the agreements between the National Research Nuclear University „MEPhI“ and JSC „All-Russian Research Institute for the Operation of Nuclear Power Plants“ dated 19.11.2019 № 00-3-700-0650 and agreement of JSC „All-Russian Research Institute for the Operation of Nuclear Power Plants“ with JSC „Science and Innovation“ dated 09.04.2019 № 313/1658-D.

### Conflict of interest

The authors declare that they have no conflict of interest.

## References

[1] P.K.F. Grieder. *Cosmic rays at Earth: researcher's reference manual and data book* (Elsevier, 2001), p. 432.
[2] L.W. Alvarez, J.A. Anderson, F.E. Bedwei, J. Burkhard, A. Fakhry, A. Girgis, A. Goneid, F. Hassan, D. Iverson, G. Lynch, Z. Miligy, A.H. Moussa, M. Sharkawi, L. Yazolino. Science, **167** (3919), 832 (1970). DOI: 10.1126/science.167.3919.832
[3] L. Bonechi, R. D'Alessandro, A. Giammanco. Rev. Phys., **5**, 100038 (2020). DOI: 10.1016/j.revip.2020.100038
[4] L. Olah, H.K.M. Tanaka, D. Varga. *Muography: Exploring Earth.s Subsurface with Elementary Particles* (John Wiley & Sons, 2022)
[5] International Atomic Energy Agency. *Muon imaging: Present status and emerging applications* (Vienna, 2022)
[6] N.S. Barbashina, R.P. Kokoulin, K.G. Kompaniets, G. Mannocchi, A.A. Petrukhin, O. Saavedra, D.A. Timashkov, G. Trinchero, D.V. Chernov, V.V. Shutenko, I.I. Yashin. Instrum. Exp. Tech., **51** (2), 180 (2008). DOI: 10.1134/S002044120802005X
[7] I.I. Yashin, N.V. Ampilogov, I.I. Astapov, N.S. Barbashina, V.V. Borog, A.N. Dmitrieva, R.P. Kokoulin, K.G. Kompaniets, G. Mannocchi, A.S. Mikhailenko, A.A. Petrukhin, O. Saavedra, V.V. Shutenko, G. Trinchero, E.I. Yakovleva. J. Phys.: Conf. Ser., **409**, 012192 (2013). DOI: 10.1088/1742-6596/409/1/012192
[8] N.V. Ampilogov, I.I. Astapov, N.S. Barbashina, V.V. Borog, A.N. Dmitrieva, A.A. Kovylyaeva, K.G. Kompaniets, A.A. Petrukhin, V.V. Shutenko, I.I. Yashin. J. Phys.: Conf. Ser., **675**, 032042 (2016). DOI: 10.1088/1742-6596/675/3/032042
[9] K. Morishima, M. Kuno, A. Nishio, N. Kitagawa, Y. Manabe, M. Moto, F. Takasaki, H. Fujii, K. Satoh, H. Kodama, K. Hayashi, S. Odaka, S. Procureur, D. Attie, S. Bouteille, D. Calvet, C. Filosa, P. Magnier, I. Mandjavidze, M. Riallot, B. Marini, P. Gable, Y. Date, M. Sugiura, Y. Elshayeb, T. Elnady, M. Ezzy, E. Guerriero, V. Steiger, N. Serikoff, J. Mouret, B. Charles, H. Helal, M. Tayoubi. Nature, **552**, 386 (2017). DOI: 10.1038/nature24647
[10] S. Procureur, K. Morishima, M. Kuno, Y. Manabe, N. Kitagawa, A. Nishio, H. Gomez, D. Attie, A. Sakakibara, K. Hikata, M. Moto, I. Mandjavidze, P. Magnier, M. Lehuraux, T. Benoit, D. Calvet, X. Coppolani, M. Kebbiri, P. Mas, H. Helal, M. Tayoubi, B. Marini, N. Serikoff, H. Anwar, V. Steiger, F. Takasaki, H. Fujii, K. Satoh, H. Kodama, K. Hayashi, P. Gable, E. Guerriero, J. Mouret, T. Elnady, Y. Elshayeb, M. Elkarmoty. Nature Commun., **14**, 1144 (2023). DOI: 10.1038/s41467-023-36351-0
[11] H.K.M. Tanaka. Phil. Trans. R. Soc. A, **377** (2137), 20180142 (2019). DOI: 10.1098/rsta.2018.0142
[12] M. D'Errico, F. Ambrosino, A. Anastasio, S. Basnet, L. Bonechi, M. Bongi, A. Bross, R. Ciaranfi, L. Cimmino, V. Ciulli, R. D.Alessandro, A. Giammanco, F. Giudicepietro, S. Gonzi, R. Karnam, G. Macedonio, V. Masone, N. Mori, M. Moussawi, M. Orazi, G. Passeggio, R. Peluso, A. Pla-Dalmau, C. Rendon, A. Samalan, G. Saracino, G. Scarpato, P. Strolin, M. Tytgat, E. Vertechi, L. Viliani. JAIS, **1**, 273 (2022). DOI: 10.31526/jais.2022.273
[13] D. Bryman, J. Bueno, K. Davis, V. Kaminski, Z. Liu, D. Oldenburg, M. Pilkington, R. Sawyer. Building Exploration Capability for the 21st Century: Society of Economic Geologists, **18**, 235 (2014). DOI: 10.5382/SP.18.11
[14] A. Lechmann, D. Mair, A. Ariga, T. Ariga, A. Ereditato, R. Nishiyama, C. Pistillo, P. Scampoli, F. Schlunegger, M. Vladymyrov. Earth-Sci. Rev., **222**, 103842 (2021). DOI: 10.1016/j.earscirev.2021.103842
[15] A. Abiev, A. Bagulya, M. Chernyavskiy, A. Dashkina, A. Dimitrienko, A. Gadjiev, M. Gadjiev, V. Galkin, A. Gippius, L. Goncharova, V. Grachev, N. Konovalova, A. Managadze, N. Okateva, N. Polukhina, T. Roganova, T. Shchedrina, N. Starkov, A. Teymurov, V. Tioukov, S. Vasina, P. Zarubin. Appl. Sci., **9** (10), 2040 (2019). DOI: 10.3390/app9102040

[16] A.B. Alexandrov, A.M. Anokhina, S.G. Vasina, A.A. Gippius, S.A. Gorbunov, V.M. Grachev, N.S. Konovalova, Yu.O. Krasilnikova, A.A. Larionov, A.K. Managadze, I.A. Melnichenko, N.M. Okateva, S.S. Paramonov, A.A. Petrukhin, N.G. Polukhina, T.M. Roganova, Zh.T. Sadykov, N.I. Starkov, E.N. Starkova, V.E. Tioukov, M.M. Chernyavskii, V.I. Shevchenko, T.V. Shchedrina. Bull. Lebedev Phys. Inst., **50**, 603 (2023). DOI: 10.3103/S1068335623120023

[17] K. Chaiwongkhot, T. Kin, H. Ohno, R. Sasaki, Y. Nagata, K. Kondo, Y. Watanabe. IEEE Transactions Nucl. Sci., **65** (8), 2316 (2018). DOI: 10.1109/TNS.2018.2855737

[18] P.M.R. Arbol, P.G. Garcia, C.D. Gonzalez, A. OrioAlonso. Phil. Trans. R. Soc. A., **377**, 20180054 (2019). DOI: 10.1098/rsta.2018.0054

[19] S. Barnes, A. Georgadze, A. Giammanco, M. Kiisk, V.A. Kudryavtsev, M. Lagrange, O.L. Pinto. Instruments, **7** (1), 13 (2023). DOI: 10.3390/instruments7010013

[20] M. Moussawi, A. Giammanco, V. Kumar, M. Lagrange. PoS., **452**, 29 (2024). DOI: 10.22323/1.452.0029

[21] J.M. Durham, D. Poulson, J. Bacon, D.L. Chichester, E. Guardincerri, C.L. Morris, K. Plaud-Ramos, W. Schwendiman, J.D. Tolman, P. Winston. Phys. Rev. Appl., **9** (4), 044013 (2018). DOI: 10.1103/PhysRevApplied.9.044013

[22] M.J. Weekes, A.F. Alrheli, D. Barker, D. Kikola, A.K. Kopp, M. Mhaidra, J.P. Stowell, L.F. Thompson, J.J. Velthuis. JINST, **16**, P05007 (2021). DOI: 10.1088/1748-0221/16/05/P05007

[23] G. Jonkmans, V.N.P. Anghel, C. Jewett, M. Thompson. Annals Nucl. Energy, **53**, 267 (2013). DOI: 10.1016/j.anucene.2012.09.011

[24] J. Perry, M. Azzouz, J. Bacon, K. Borozdin, E. Chen, J. Fabritius, E. Milner, H. Miyadera, C. Morris, J. Roybal, Z. Wang, B. Busch, K. Carpenter, A.A. Hecht, K. Masuda, C. Spore, N. Toleman, D. Aberle, Z. Lukic. J. Appl. Phys., **113**, 184909 (2013). DOI: 10.1063/1.4804660

[25] B. Lefevre, H. Gomez, S. Procureur, D. Attie, L. Gallego, P. Gonzales, M. Lehuraux, B. Lesage, I. Mandjavidze, P. Mas, D. Pomarede. EPJ Web Conf., **288**, 07001 (2023). DOI: 10.1051/epjconf/202328807001

[26] H. Miyadera, K.N. Borozdin, S.J. Greene, Z. Lukic, K. Masuda, E.C. Milner, C.L. Morris, J.O. Perry. AIP Advances, **3**, 052133 (2013). DOI: 10.1063/1.4808210

[27] N. Kume, H. Miyadera, C.L. Morris, J. Bacon, K.N. Borozdin, J.M. Durham, K. Fuzita, E. Guardincerri, M. Izumi, K. Nakayama, M. Saltus, T. Sugita, K. Takakura, K. Yoshioka. JINST, **11**, P09008 (2016). DOI: 10.1088/1748-0221/11/09/P09008

[28] H. Fujii, M. Gi, K. Hara, S. Hashimoto, K. Hayashi, H. Kakuno, H. Kodama, M. Mizokami, S. Mizokami, K. Nagamine, K. Sato, S. Sekita, H. Shirai, S. Kim, T. Sumiyoshi, A. Suzuki, Y. Takada, K. Takahashi, Y. Takahashi, F. Takasaki, D. Yamada, S. Yamashita. Prog. Theor. Exp. Phys., **2021** (2), 023C01 (2021). DOI: 10.1093/ptep/ptaa137

[29] N.S. Barbashina, V.V. Borog, R.P. Kokoulin, K.G. Kompaniets, A.A. Petrukhin, D.A. Timashkov, V.V. Shutenko, I.I. Yashin. *Method and apparatus for obtaining muonographs* (Patent RU2406919C2 dated 20.12.2010, Federal Institute of Industrial Property, URL: https://patentimages.storage.googleapis.com/4e/6d/b5/12929dad5e5150/RU2406919C2.pdf)

[30] I.I. Astapov, M.M. Kaverznev, Yu.N. Konev, A.A. Petrukhin, S.S. Khokhlov, I.I. Yashin. *Muon hodoscope and device for diagnostics of objects* (Patent RU2761333C1 dated 07.12.2021 Federal Institute of Industrial Property, URL:https://www1.fips.ru/ofpstorage/Doc/IZPM/RUNWC1/000/000/002/761/333/%D0%98%D0%97-02761333-00001/document.pdf)

[31] N.A. Pasyuk, A.A. Borisov, K.G. Kompaniets, A.S. Kozhin, R.M. Fakhrutdinov, M.Yu. Tselinenko, V.V. Shutenko, I.I. Yashin. Instrum. Exp. Tech., **67** (2), 219 (2024). DOI: 10.1134/S0020441224700489

[32] N.A. Pasyuk, K.G. Kompaniets, A.A. Petrukhin, M.Yu. Tselinenko, V.V. Shutenko, I.I. Yashin. PTE: accepted for publication on 06.12.2023. DOI(preprint): 10.13140/RG.2.2.21424.53762

[33] A.A. Borisov, M.Yu. Bogolyubsky, N.I. Bozhko, A.N. Isaev, A.S. Kozhin, A.V. Kozelov, I.S. Plotnikov, V.A. Senko, M.M. Soldatov, R.M. Fakhrutdinov, N.A. Shalanda, O.P. Yushchenko, V.I. Yakimchuk. PTE, **2**, (in Russian). 5 (2012).

[34] I.I. Yashin, V.V. Kindin, K.G. Kompaniets, N.N. Pasyuk, M.Yu. Tselinenko. Bull. Russ. Academ. Sci.: Phys., **85**, 458 (2021). DOI: 10.3103/S1062873821040389

[35] N.A. Pasyuk, N.N. Davidenko, A.S. Kozhin, K.G. Kompaniets, Yu.N. Konev, S.V. Oleinik, A.A. Petrukhin, R.M. Fakhrutdinov, M.Yu. Tselinenko, D.V. Shudra, V.V. Shutenko, I.I. Yashin. ZhTF, **94** (8), 1398 (2024) (in Russian). DOI: 10.61011/JTF.2024.08.58569.40-24

[36] Electronic source. Website of NPP LLC „Hangar Systems“, URL: https://nebo-chel.ru/naduvnye-sooruzhenija/pnevmokarkasnye-moduli

[37] J. Chen, H. Li, Y. Li, P. Liu. JINST, **18**, P08008 (2023). DOI: 10.1088/1748-0221/18/08/P08008

[38] M. Guan, M.C. Chu, J. Cao, K.B. Luk, C. Yang. *A parametrization of the cosmic-ray muon flux at sea-level*, arXiv:1509.06176 (2015). DOI: 10.48550/arXiv.1509.06176

*Translated by A.Akhtayamov*